A Microgravity Emulation Testbed for Asteroid Exploration Robots

Marco Chacin and Kazuya Yoshida
Department of Aerospace Engineering, Tohoku University
Aoba 6-6-01, Sendai, 980-8579, JAPAN
{mchacin, yoshida}@astro.mech.tohoku.ac.jp

Abstract

In this paper, the development of a microgravity emulator intended to be a test field for future asteroid exploration rovers is presented. The proposed control methods are validated using hardware-in-the-loop simulations. Experiments are performed with a multi-limbed robot attached to a manipulator's end tip under emulated microgravity conditions. This analysis plays a fundamental step towards the development of next generation space robots capable of landing smoothly on an asteroid, and will be beneficial for producing control algorithms that can make them move in a stable fashion while remaining attached to the surface against the dynamic reaction from the moving limbs.

1. Introduction

During the last decade there has been an increased scientific interest in exploring the asteroids of the solar systems. Some of the reasons of this interest are possible scientific discoveries that may help to understand the formation of the Earth, the threat of asteroid collision with our planet, and the potential existence of valuable resources. These reasons have pushed recent technological advances that enable mankind for the first time to take a closer look at these small solar system objects. The exploration of asteroids began back in 1991 with Galileo's flyby of the Gaspra asteroid[1] and have continued since then with additional missions like the Near Earth Asteroid Rendezvous (NEAR Shoemaker) mission[2] to 433 Eros. One of the latest of these space probes, the Japanese Hayabusa [3](Fig.1), successfully orbited and mapped the Itokawa asteroid in 2005. The spacecraft was intended to touchdown[4] on Itokawa and return with ground samples back to Earth. The current flagship mission for asteroid exploration is the NASA Dawn mission launched in September 2007, which will investigate two of the largest bodies in the main asteroid belt, Vesta and Ceres.

The Hayabusa mission carried onboard a small "hopping robot" named MINERVA[5] to be deployed and used to explore the asteroid surface and transmit the data back to its mother ship. Although, the robot was not successfully deployed, it was intended to use a single reaction wheel (located inside the robot) to produce the necessary inertial reaction to move. But with this system the location of the robot when the bounds are finally damped out is very challenging to predict or control.

Since 2003, the Space Robotics Laboratory at Tohoku University has been developing the next generation of asteroid explorer systems. A proposed solution uses a multi-limbed robot, which is henceforth referred to as ASTRO (ASTeroid RObot). The development of this robot is part of a bigger scheme, where a platform for teleoperated space exploration robots[6] is developed. This platform includes a test field where the commanded motions of the robot can be tested in advance to accurately predict its actual behavior and to verify that the desired series of movements can be accomplished by the hardware without risking the mission. To assess these requirements a system must be developed to emulate the microgravity conditions found on an asteroid.

In this paper, the development of a control system that uses a robotic manipulator arm equipped with a Force/Torque sensor on its end tip to emulate microgravity is presented. By taking into account the contact dynamics of the robot with the surface and its reaction forces the system can accurately counterbalance the Earth's gravity pull, limited by the manipulator's workspace. Experiments are performed to show how proper selections of parameter values lead to a manipulator behavior suitable for emulating microgravity. The proposed control methods are validated using hardware-in-the-loop simulations performed under emulated microgravity conditions, with a multi-limbed robot attached to the manipulator end tip.

2. Asteroid Exploration

Orbiting between 2.1 to 3.2 AU[1] from our sun, primitive asteroids represent key bodies to research on the early planetary system origin and evolution. They are small rocky bodies with no atmosphere and are believed to be remnants

[1] *AU stands for astronomical unit and is based on the mean distance from Earth to the Sun, 9.3×10^7 miles (1.5×10^8 km).*

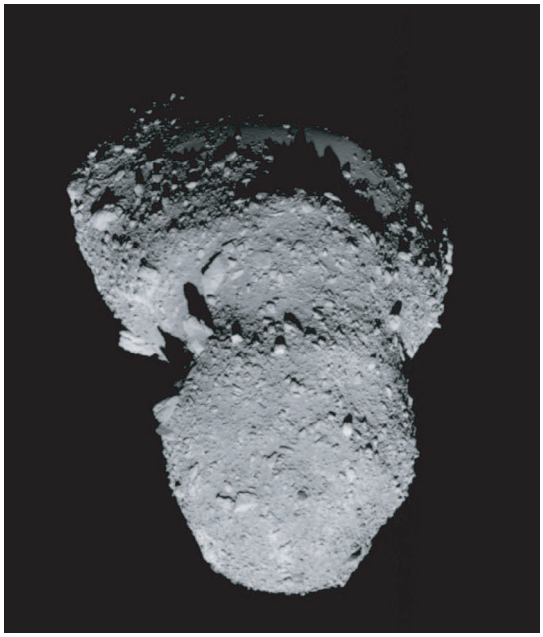

Figure 1. Asteroid 25143 Itokawa surface photo. ©JAXA/ISAS

that date as old as the formation of our solar system. Beyond their size, shape and rotation relatively little is known about these objects. Since they could provide clues about the birth and growth of our planetary system, scientists have catalogued asteroids in more than a dozen spectral classes based on their albedo[2], but without any in-situ observation, they are not able to link this catalog with a corresponding meteorite group. The in-situ study of asteroids can lead to important scientific findings, in the effort to map the asteroid belt. Mapping the asteroid belt by spectral classes and also knowing from which region the meteorites on Earth come from can provide key clues about the origin and evolution of our solar system, even including the geological history of our planet Earth [7].

Asteroids' physical characteristics provide a very hostile environment distinguished by the absence of almost any gravity. The effects of the microgravity environment can be approximated for convenience as those in the level of $10^{-6}G$ [8]. In such an environment, objects basically do not fall, but remain orbiting unless they reach the low escape velocity of the asteroid in the order of 2×10^{-4} [km/s], as in the case of the asteroid 25143 Itokawa[8]. To attain stable mobility in these bodies, it is critical to consider the forces interaction between a robot and the asteroid's surface in this microgravity environment. Therefore, moving on asteroids would require proper stability control against

[2]*Albedo is the ratio of reflected to incident electromagnetic radiation. It is a dimensionless measure indicative of a surface's or body's diffuse reflectivity. The albedo of planets, satellites and asteroids can be used to infer much about their properties.*

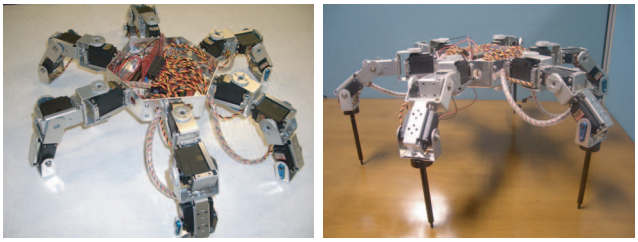

Figure 2. Rover during early stages of development.

the forces interacting between bodies in microgravity environment to increase any scientific return from the mission operating on the asteroid surface.

3. Asteroid Robot (ASTRO)

In a future asteroid exploration mission[9][10][11], a smart design of a robotic system that would allow scientists more accurate positioning on the microgravity environment is expected. A small limbed robot would be deployed over the asteroid to crawl on its rough surface.

The asteroid robot (ASTRO) is a multi-limbed ambulatory locomotion system[12] developed through the observation and mimetic of clever solutions exhibited by biological systems. During its development, the limbed robot concept has been inspired from nature to obtain a platform complexity with a type of mechanism expected to perform robustly in unstructured environments, through the replication of walking gates using six limbs, like arachnid insects. The use of six legs was decided based on the needs of a mission to an asteroid, where the microgravity environment would impose on the robot the challenging task of moving with high accuracy and still performing science operations in a stable manner. The main purpose of this form of motion is to avoid getting ejected from the surface. Therefore, six legs would be of better use than two or four, given the possibility of using at least three limbs to grasp the surface to maintain the robot attached to the asteroid as a stable base while still using the remaining limbs for locomotion towards any direction or available for manipulation. For this reason, ASTRO is equipped with Force/Torque sensors on its end tips to provide feedback of the applied force to the surface.

ASTRO is expected to land on an asteroid and have the ability of fine positioning over the surface to achieve science studies and mapping at several locations. As a result, the robot's design has been developed in a modular basis for all of its components, facilitating any normal changes in the adaptation process to accomplish a robust design for the demanding activities imposed by a mission to an asteroid, starting from the most critical part of the mission: the

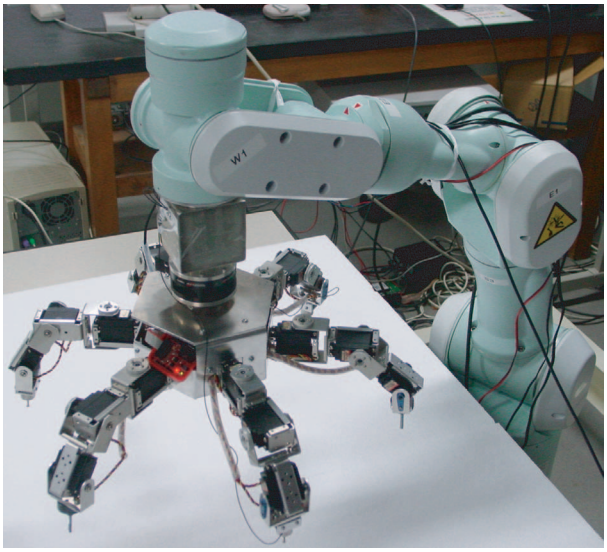

Figure 3. ASTRO attached to the manipulator arm and the F/T sensor.

landing phase. Furthermore, power[3], communication, intelligent control and other housekeeping functions must all be contained within the robot to permit for autonomous operation.

4. Emulating Microgravity

To simulate the real dynamic conditions of robot over an asteroid, the authors used a robust control system that could counterbalance Earth's gravity and leave the robot in an emulated state of microgravity. For this reason, ASTRO was mounted on the tip of a Mitsubishi PA10 manipulator arm (Fig.3) controlled by a dynamics based model simulation equipped with a ATI Industrial Automation Gamma SI-32-2.5 Force/Torque sensor[13]. The configuration was setup to perform further experiments with the robot to observe and analyze its behavior under microgravity conditions, as it would approach the surface of an asteroid prior to touchdown.

Gravity emulation is achieved through impedance control, also known as virtual compliance control, as shown in [14]. The control algorithm is based upon the basic equation of motion shown in (1).

$$[\boldsymbol{m}]\frac{\boldsymbol{d\overline{v}}}{\boldsymbol{dt}} = \overline{\boldsymbol{q}} - [\boldsymbol{K}]\Delta\overline{\boldsymbol{x}} - [\boldsymbol{C}]\overline{\boldsymbol{v}} \tag{1}$$

where $\overline{\boldsymbol{q}}$ is the external force and torque applied to the end tip, $\Delta\overline{\boldsymbol{x}}$ is the displacement of the end tip relative to the reference and $\overline{v}$ is its velocity. $[\boldsymbol{m}] \in R^6$ is the virtual mass, $[\boldsymbol{K}] \in R^6$ is the virtual spring constant and $[\boldsymbol{C}] \in R^6$ is the damping constant. (1) can be transformed into

$$\overline{\boldsymbol{v}} = \frac{1}{[\boldsymbol{m}]}\int(\overline{\boldsymbol{q}} - [\boldsymbol{K}]\Delta\overline{\boldsymbol{x}} - [\boldsymbol{C}]\overline{\boldsymbol{v}})\boldsymbol{dt} \tag{2}$$

which can be represented as the following finite differential equation

$$\overline{\boldsymbol{v}}_n = \frac{\boldsymbol{\Delta t}}{[\boldsymbol{m}]}(\overline{\boldsymbol{q}}_{n-1} - [\boldsymbol{K}]\boldsymbol{\Delta}\overline{\boldsymbol{x}}_{n-1}) + ([\boldsymbol{I}] - \frac{\boldsymbol{\Delta t}}{[\boldsymbol{m}]}[\boldsymbol{C}])\overline{\boldsymbol{v}}_{n-1} \tag{3}$$

where $\boldsymbol{\Delta t}$ is the time step and $[\boldsymbol{I}]$ is the identity matrix. (3) describes the velocity at the sampling time based upon values from the previous time step. Based on this equation, and knowing the forces and torques as well as the displacement of the arm, it can be controlled in real-time using (3) and (4). In short, the control policy uses the relationship between force and velocity to find the position and then calculate a velocity command as input to the system. The behavior of the system can be altered by changing the impedance constants $[\boldsymbol{m}]$, $[\boldsymbol{K}]$ and $[\boldsymbol{C}]$ which can be fine tuned in order to exhibit the desired properties. The estimation of these parameters is detailed in forthcoming sections.

4.1. Dynamic Model

The dynamic motion of the free-flying multi-body system with the presence of the external forces $\boldsymbol{F}_{ex}$ is described as [15]:

$$\boldsymbol{H}\begin{bmatrix}\ddot{\boldsymbol{x}}_b \\ \ddot{\boldsymbol{\phi}}\end{bmatrix} + \begin{bmatrix}\boldsymbol{c}_b \\ \boldsymbol{c}_m\end{bmatrix} = \begin{bmatrix}\boldsymbol{F}_b \\ \boldsymbol{\tau}\end{bmatrix} + \boldsymbol{J}^T\boldsymbol{F}_{ex} \tag{4}$$

where,

$\boldsymbol{H}$	: inertia matrix of the robot
$\boldsymbol{x}_b$	: position/orientation of the base
$\boldsymbol{\phi}$	: articulated joint angles
$\boldsymbol{c}_b, \boldsymbol{c}_m$	: velocity/gravity dependent non-linear terms
$\boldsymbol{F}_b$	: forces/moments directly apply on the base
$\boldsymbol{\tau}$	: joint articulated torque
$\boldsymbol{J}^T$	: Jacobian matrix
$\boldsymbol{F}_{ex}$	: external forces/moments on the end points

And the kinematic relationship around the end points is expressed as follows:

$$\dot{\boldsymbol{x}}_{ex} = \boldsymbol{J}_m\dot{\boldsymbol{\phi}} + \boldsymbol{J}_b\dot{\boldsymbol{x}}_b \tag{5}$$

$$\ddot{\boldsymbol{x}}_{ex} = \boldsymbol{J}_m\ddot{\boldsymbol{\phi}} + \dot{\boldsymbol{J}}_m\dot{\boldsymbol{\phi}} + \boldsymbol{J}_b\ddot{\boldsymbol{x}}_b + \dot{\boldsymbol{J}}_b\dot{\boldsymbol{x}}_b \tag{6}$$

where the $\boldsymbol{J}_b$ and $\boldsymbol{J}_m$ denote the Jacobian of the base (main) body and the Jacobian of a given manipulator (limb) respectively.

The magnitude of the forces is determined by the friction of the contact surface. Let us consider the i-th limb of the

[3] *Power sources like batteries had not been fully integrated on the robot at the time of this writing.*

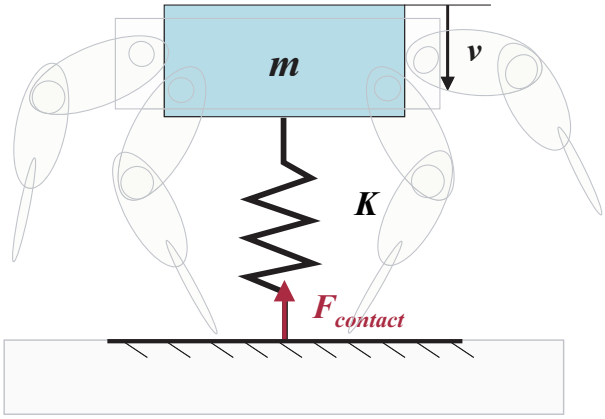

Figure 4. Landing model.

robot. $\boldsymbol{p}_{ij} \in R^{3\times1}$, $\boldsymbol{f}_{ij} \in R^{3\times1}$ and $\boldsymbol{\tau}_{ij} \in R^{3\times1}$ denote the contact position vector, the contact force and the joint torque vector, respectively, i and j express the i-th limb and the j-th contact point. Let $\boldsymbol{\tau}_i^j$ be the torque due to the contact force $\boldsymbol{f}_{ij}$. The relationship between the contact force and the joint torque is given by

$$\boldsymbol{\tau}_i^j = \boldsymbol{J}_{ij}^T \boldsymbol{f}_{ij} \tag{7}$$

where $\boldsymbol{J}_{ij}^T$ denotes the transpose of the Jacobian matrix that maps the contact force into the joint torque. Then, using the principle of superposition for the relationship between $\boldsymbol{\tau}_i^j$ and $\boldsymbol{f}_i$, we have:

$$\boldsymbol{\tau}_i = \sum_{j=1}^{k_i} \boldsymbol{\tau}_i^j \tag{8}$$

$$\boldsymbol{\tau}_i = \sum_{j=1}^{k_i} \boldsymbol{J}_{ij}^T \boldsymbol{f}_i \tag{9}$$

here, k_i is the number of contact points of the i-th limb. Since it is assumed that a limb can only have one contact point, (9) can be rewritten in the following form.

$$\boldsymbol{\tau}_i = \boldsymbol{J}_i^T \boldsymbol{f}_i \tag{10}$$

where $\boldsymbol{\tau}_i = [\boldsymbol{\tau}_{i1}, \cdots, \boldsymbol{\tau}_{im}]^T$, $\boldsymbol{f}_i = [\boldsymbol{f}_{i1}^T, \cdots, \boldsymbol{f}_{im}^T]^T$ and $\boldsymbol{J}_i^T = [\boldsymbol{J}_{i1}^T, \cdots, \boldsymbol{J}_{im}^T]$.

4.2. Compliance and stiffness

Given an applied force on the end tip, the kinematic chain (on any given limb) experiences a deformation. The relation between the applied force and the corresponding deformation is defined as the "stiffness" of the kinematic chain. This stiffness can be related to two possibilities: the mechanical elasticity of the system and/or the dynamic behavior of the control system.

In general, for each joint exists a deflexion component defined by:

$$\boldsymbol{\tau} = \boldsymbol{K}\Delta\boldsymbol{\phi} \tag{11}$$

where

$$\boldsymbol{K} = \begin{bmatrix} \boldsymbol{k}_1 & & 0 \\ & \ddots & \\ 0 & & \boldsymbol{k}_N \end{bmatrix} \tag{12}$$

The relation between the force $\boldsymbol{f}_i$ and the corresponding spatial deformation $\Delta\boldsymbol{p}$ is:

$$\Delta\boldsymbol{p} = \boldsymbol{J}\Delta\boldsymbol{\phi} \tag{13}$$

Solving (11) for $\Delta\boldsymbol{\phi}$,

$$\Delta\boldsymbol{\phi} = \boldsymbol{K}^{-1}\boldsymbol{\tau} \tag{14}$$

And substituting in (13),

$$\Delta\boldsymbol{p} = \boldsymbol{J}\boldsymbol{K}^{-1}\boldsymbol{\tau} \tag{15}$$

Finally, from (10) and (15),

$$\Delta\boldsymbol{p} = \boldsymbol{J}\boldsymbol{K}^{-1}\boldsymbol{J}^T\boldsymbol{f}_i \tag{16}$$

From this point the compliance matrix can be defined as:

$$\boldsymbol{C} = \boldsymbol{J}\boldsymbol{K}^{-1}\boldsymbol{J}^T \tag{17}$$

On the other hand, the impact phase can be divided in two stages, compression and restitution. During the compression stage the elastic energy is absorbed by the deformation of the contact surfaces of the impacting bodies. In the restitution stage the elastic energy stored in compression is released back to the bodies making the relative velocity greater than zero.

Therefore, the robot can be modeled as a mass-spring system(Fig.4) with a purely elastic contact at its end tips. Therefore, the following relation between the mass, the velocity and the force should hold:

$$2\boldsymbol{m}\boldsymbol{v} = \boldsymbol{F}\Delta\boldsymbol{t} \tag{18}$$

Isolating the reaction force, we have:

$$\boldsymbol{F} = \frac{2\boldsymbol{m}\boldsymbol{v}}{\Delta\boldsymbol{t}} \tag{19}$$

Now, considering the time of contact as a function of the mass of the system $\boldsymbol{m}$ and the stiffness coefficient of the limbs $\boldsymbol{K}$, we have:

$$\Delta\boldsymbol{t} = \pi\sqrt{\frac{\boldsymbol{m}}{\boldsymbol{K}}} \tag{20}$$

Finally, from (19) and (20),

$$\boldsymbol{F}_{contact} = \frac{2}{\pi}\left(\sqrt{\boldsymbol{m}\boldsymbol{K}}\right)\boldsymbol{v} \tag{21}$$

with

$$\boldsymbol{F}_{contact} = \sum_{i=1}^{N} \boldsymbol{f}_i \tag{22}$$

where N is the number of limbs in contact at landing.

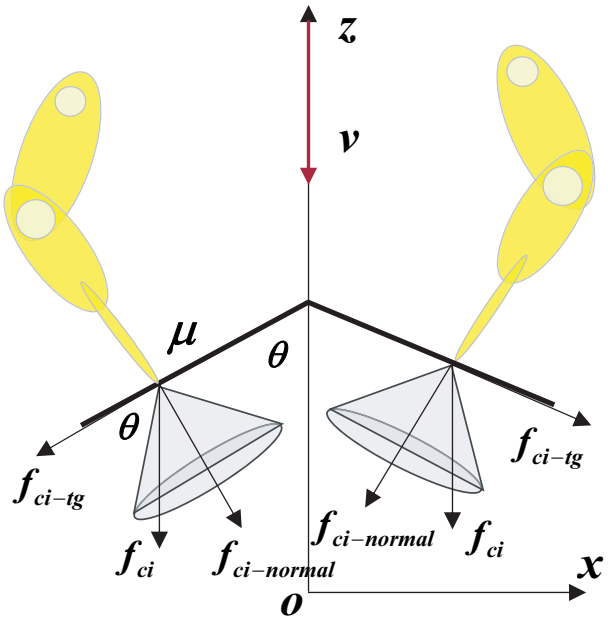

Figure 5. Decomposition of the contact forces.

4.3. Contact Dynamics

In commonly used contact models, it is observed that as the stiffness coefficient is lowered, greater penetration in the ground occurs. The lower the damping constants are, the longer the vibrations occur. However, a very high increment in stiffness or in damping constants can produce instabilities in simulations due to numerical issues.

The following discussion is on how to determine the contact force $\boldsymbol{F}_{ex}$[16]. In literature [17][18] the relationship of momentum exchange and force-time product assumes infinitesimal impact. However, the infinitesimal impact between two single rigid bodies is a much idealized case. If the colliding body has elasticity, there eventually occurs non-zero, finite-time period of contact. Or, if the system is articulated and the connecting joints are compliant[19], the methods discussed for infinitesimal impact of a single rigid body cannot be applied. We may call such finite-time contact as *soft* contact against the infinitesimal impact as *hard* contact.

Since the authors assume a model with a purely elastic deformation in the normal ($\boldsymbol{z}$) direction of the contact point, and Coulomb friction in the tangential directions[20][21], we have the following general expressions from Fig.5:

$$\boldsymbol{f}_{ci-tg} = \boldsymbol{f}_{ci} cos\theta \quad (23)$$

$$\boldsymbol{f}_{ci-normal} = \boldsymbol{f}_{ci} sin\theta \quad (24)$$

where $\boldsymbol{\theta}$ is the angle of the surface normal.

Next, the coefficient of friction can be noted as:

$$\boldsymbol{\mu} = \frac{\boldsymbol{f}_{ci}}{\boldsymbol{f}_{ci-normal}} > \frac{\boldsymbol{f}_{ci} cos\theta}{\boldsymbol{f}_{ci} sin\theta} \quad (25)$$

$$\boldsymbol{\mu} > \boldsymbol{f}_{ci} tan\theta \quad (26)$$

Considering $\boldsymbol{F}_{contact} = \boldsymbol{f}_{ci}$ on the last expression, and using (19) we have,

$$\boldsymbol{\mu} > \frac{2\boldsymbol{m}\boldsymbol{v}}{\Delta \boldsymbol{t}} tan\theta \quad (27)$$

And substituting (20),

$$\frac{tan\theta \boldsymbol{\mu}}{2\boldsymbol{m}} \left(\pi \sqrt{\frac{\boldsymbol{m}}{\boldsymbol{K}}} \right) > \boldsymbol{v} \quad (28)$$

(28) shows that the considered contact stability will strictly depend on the approach velocity of the robot.

Although, quasi-static stability is a more general stability criterion than that used in the previous discussion. Under this condition inertia forces are included but limb dynamics are not separately considered, the masses of the limbs being lumped with that of the body. However, the in the previous argument, quasi-static stability is, partly, assumed provided all the normal components of the contact points forces are positive. Since the contact point cannot support a negative normal force (as shown in Fig.5), the appearance of a negative force indicates that the given limb will lift and, since it cannot provide the required movement about the center of mass, the robot will jump in a microgravity environment.

5. Experimental Results

To evaluate the performance of the control strategy a several of tests were designed to examine how the impedance constants $[\boldsymbol{m}]$, $[\boldsymbol{K}]$ and $[\boldsymbol{C}]$ influence the behavior of the system. For the sake of simplicity, only four typical cases are described while keeping $[\boldsymbol{m}]$ constant to damp out small mechanical vibrations on the system.

During the first case the parameters selected under the following constraint $\boldsymbol{K} \gg \boldsymbol{C}$. A force is applied on the manipulator's end tip, which is displaced before it starts swinging back and forth. A small reduction in the position is observed with time since the damping is not zero.

In the second case the condition changes to as $\boldsymbol{K} > \boldsymbol{C}$. Like in the first experiment the end tip starts to swing back and forth when a force is applied, but since the damping constant $[\boldsymbol{C}]$ has been increased, this swing motion soon dies out much faster as the end tip is back to its initial position without any further movement.

For the third case, the condition is switched to $\boldsymbol{K} \ll \boldsymbol{C}$. When a force is applied, the velocity increases but it is quickly reduced back to zero. The position also exhibits a rather small change where it remains when the velocity is damped out.

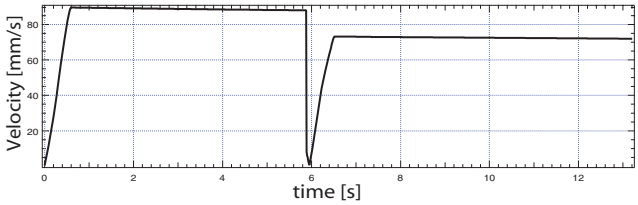

Figure 6. Composite velocity profile.

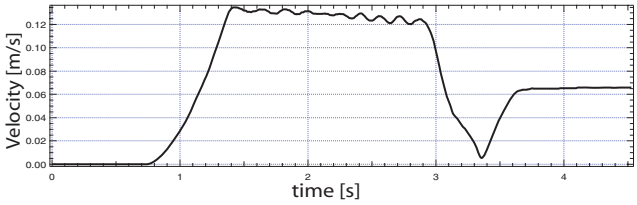

Figure 8. Body velocity.

In the fourth case, the spring and damping constants are selected to satisfy $\boldsymbol{K} < \boldsymbol{C}$, but both parameters are chosen similar to what they are expected to be in a microgravity environment, where both $[\boldsymbol{K}]$ and $[\boldsymbol{C}]$ tend to zero[4]. It was observed that the manipulator's end tip velocity changes rapidly, and then it slowly decreases its velocity due to the small damping coefficient.

Next, several tests designed to verify the energy absorption and the velocity profile of the manipulator arm were performed. A typical experimental result of one of these tests is shown in Fig.6.

It can be observed that the manipulator's end tip velocity changes after impacting the surface but remains within 10%-15% of its approaching phase yielding reasonable results that are in accordance with what is expected in microgravity conditions. At this point, if the virtual mass value is to be changed in any of the experiments, the behavior of the system would not change, but the force required in order to get the same velocity and position displacement would have increased accordingly.

After achieving a satisfactory response from the control system, ASTRO was attached to the end tip of the manipulator and was suspended above a table that serves as the landing surface shown in Fig.7. In order to have a smooth landing the robot's limbs are made compliant with the reaction forces that act on them.

From Fig.8, it can be seen that the robot is given an initial velocity to move down towards the surface. When the surface is hit (at 3.2 [s]) the reaction results in a velocity in the opposite direction making the robot leave the surface. It is observed that the rebound velocity is lower than the velocity of the impact (absolute value) with (~ 0.13 $[m/s]$ vs. ~ 0.07 $[m/s]$). The reason behind this is that some of the force is absorbed when the rover's limbs move during touchdown (as observed during the experiment). A small angular rotation occurs as the limbs on different sides of ASTRO move differently at the impact. The shock against the surface produces a low energetic reaction that rejects the rover into space with a low reactive force.

The results of this experiment suggest that when the robot performed a soft landing with no force on the limbs as some sort of suspension, almost half of the shock energy was absorbed by the movement of the limbs.

[4] *In reality* $[\boldsymbol{C}]$ *is chosen to be* 0.1 *to avoid problems in the computational solution of (3) and to satisfy the condition.*

6. Conclusions

The microgravity emulator test bed was successfully developed and implemented as a hardware-in-the-loop simulation using a robotic manipulator controlled with impedance control with feedback from a Force/Torque sensor located at the manipulator's end tip.

Experiments were performed showing how proper selections of impedance values lead to a manipulator behavior suitable for emulating microgravity. Experiments show expected results and the attached robot move and behaves as if it were in the emulated environment. The microgravity emulator can be used for future robot experiments, and in particular used for identifying desirable robot patterns for limbed robots.

A future asteroid exploration mission was considered as a specific application target.

7. Future Work

The immediate step is to use the emulator to find proper motion patterns and identify landing strategies. One possible direction for future work would be to perform experiments with a lower virtual mass, closer to the robots real mass. In order to enable this, mechanical modifications must be done to address the vibrations of the system. Two solutions are clear; to replace the current F/T sensor and ASTRO's interface with a more rigid interface and reduce the distance between the end tip and ASTRO. However, the second option can only be done by replacing the current F/T sensor with one that can attach directly to the manipulator without a custom interface.

References

[1] http://www.jpl.nasa.gov/news/fact_sheets/galileo0309.pdf

[2] NASA/JPL and JHU/APL, "Near Earth Asteroid Rendezvous Mission," *http://near.jhuapl.edu*

[3] http://www.hayabusa.isas.jaxa.jp/

[4] K. Yoshida, T. Kubota, S. Sawai, A. Fujiwara, M. Uo, "MUSES-C Touch-down Simulation on the Ground", *In AAS/AIAA Space Flight Mechanics Meeting, Paper AAS 01-135,* Santa Barbara, California, February 2001.

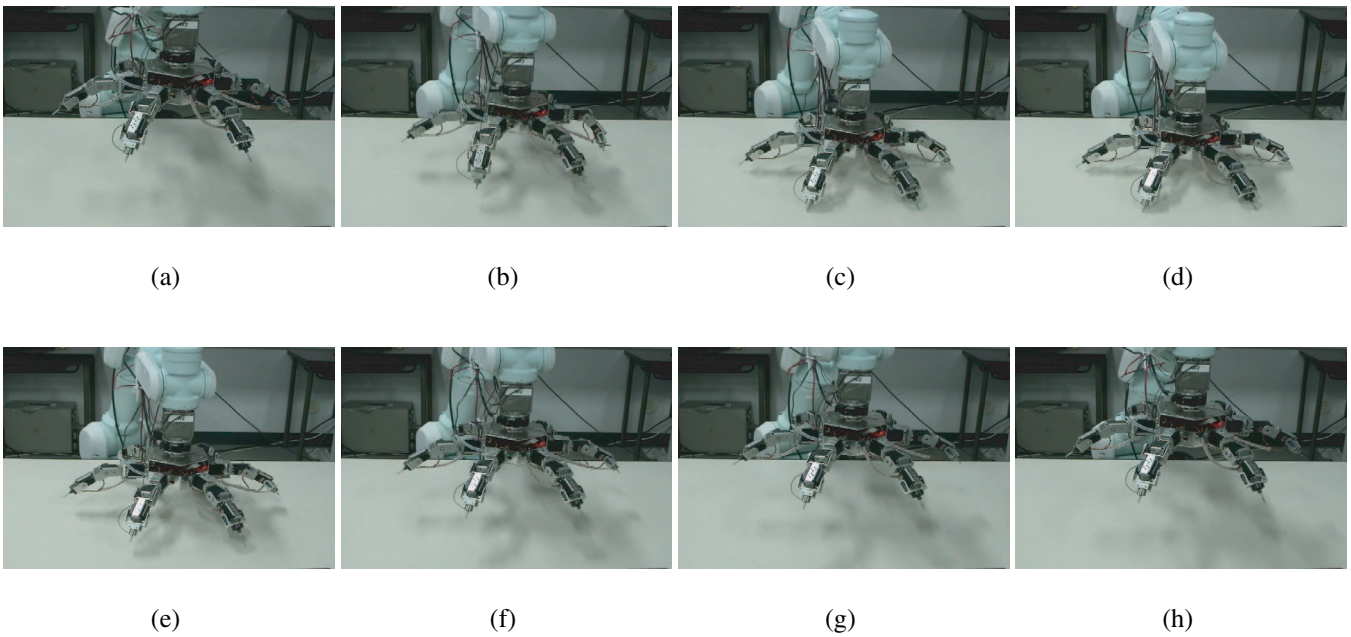

(a) (b) (c) (d)

(e) (f) (g) (h)

Figure 7. Landing on flat surface.

[5] T. Yoshimitsu, et al. "Autonomous Navigation and Observation on Asteroid Surface by Hopping Rover MINERVA," *In Proc. 6th Int. Symp. on Artificial Intelligence and Robotics & Automation in Space, i-SAIRAS 2001,* Canadian Space Agency, Quebec, Canada, June 2001 (CD-ROM).

[6] M. Chacin, A. Mora, E. Rohmer and K. Yoshida, "A High Level Teleoperation Platform for Space Robotic Missions," *Proceedings of the 2nd International Conference on Space Mission Challenges for Information Technology (SMC-IT),* pp.133-139, Pasadena, USA, 2006.

[7] A. Fujiwara, J. Kawaguchi, D. K. Yeomans et al. "The Rubble Pile Asteroid Itokawa as observed by Hayabusa. Report: Hayabusa at asteroid Itokawa," *Science,* vol. 312, 2006.

[8] D. Scheeres, "Dynamical Environment About Asteroid 25143 Itokawa," University of Michigan, Department of Aerospace Engineering, USA.

[9] M. Chacin, and K. Yoshida; " Multi-Limbed Rover for Asteroid Surface Exploration Using Static Locomotion," *In Proc. of International Symposium on Artificial Intelligence, Robotics, Automation in Space (i-SAIRAS05),*, ESA, Munich, Germany, pages. 1-8, 2005.

[10] M. Chacin and K. Yoshida, "Evolving Legged Rovers for Minor Body Exploration Missions," *Proceedings of the 1st IEEE / RAS-EMBS International Conference on Biomedical Robotics and Biomechatronics, BioRob2006,* Pisa, Italy, February, 2006.

[11] K. Yoshida, T. Maruki and H. Yano; "A Novel Strategy for Asteroid Exploration with a Surface Robot," *In Proc. of the 3rd International Conference on Field and Service Robotics,* Finland, 281-286, June, 2002.

[12] M. Chacin, K. Nagatani and K. Yoshida, "Next-Generation Rover Development for Asteroid Surface Exploration: System Description". *In Proceedings of the 25th International Symposium on Space Technology and Science and 19th International Symposium on Space Flight Dynamics,* Kanazawa, Japan, 2006.

[13] ATI Industrial Automation, "Force Torque Transducer TWE F/T Instalation and oparation manual," Component data sheet, available from ATI Industrial Automation, 2005.

[14] H, Hirabayashi, K. Sugimoto, A. Enomoto, I. Ishimaru. "Robot Manipulation Using Virtual Compliance Control," *In Journal of Robotics and Mechatronics, Vol.12, No.5,* pp. 567-575, 2000.

[15] K. Yoshida. "A General Formulation for Under-Actuated Manipulators," *Proc. 1997 IEEE/RSJ Int. Conf. on Intelligent Robots and Systems,* pp.1651-1957, Grenoble, France, 1997.

[16] A. V. Der Stappen, C. Wentink and M. Overmars, "Computing form-closure configurations," *In Proceedings of the IEEE International Conference on Robotics and Automation, ICRA* pp. 1837-1842, USA, 1999.

[17] R. M. Brach, "Mechanical Impact Dynamics: Rigid Body Collisions," John Wiley & Sons, 1991.

[18] J. B. Keller, "Impact With Friction," *ASME J. of Applied Mechanics,* vol.53, no.1, 1986.

[19] D.P.C. Klein and R. Briggs, "Use of compliance in the control of legged vehicles," *IEEE Transactions on Systems, Man and Cybernetics,* 10(7):393-400, 1980.

[20] K. Yoshida, "Touch-Down Dynamics Simulation of MUSES-C with a Contact Friction Model," *In Proceedings of 9th Workshop on Astrodynamics and Flight Mechanics,* JAXA, Kanagawa, Japan, 1999.

[21] G. Gilardi and I. Shraf, "Literature Survey of Contact Dynamics Modeling," Mechanism and Machine Theory 37, pp.1213-1239, 2002.